ECCOMAS Congress 2016
VII European Congress on Computational Methods in Applied Sciences and Engineering
M. Papadrakakis, V. Papadopoulos, G. Stefanou, V. Plevris (eds.)
Crete Island, Greece, 5–10 June 2016

A STABLE AND CONSERVATIVE TIME-DEPENDENT INTERFACE FORMULATION ON SUMMATION-BY-PARTS FORM: AN INITIAL INVESTIGATION

Samira Nikkar and Jan Nordström

Department of Mathematics, Computational Mathematics, Linköping University
SE-581 83 Linköping, Sweden
e-mail: {samira.nikkar, jan.nordstrom}@liu.se

Keywords: Time-dependent interface, Summation-by-parts, Deforming domains, Stability, Conservation, Multi-blocks.

Abstract. *A time-dependent coupling for curved multi-domain problems is considered. First, we transform the problem from Cartesian coordinates into curvilinear coordinates and apply the energy method to derive well-posed and conservative interface conditions.*

Next, we discretize the problem in space and time by employing finite difference operators that satisfy the summation-by-parts convention. The boundary and interface conditions are imposed weakly by using the simoultaneous approximation term technique as penalty formulations. The discrete version of the energy method is used to derive the stability and conservation requirements. We show how to formulate the penalty operators in such a way that the interface procedure is automatically adjusted to the movements and deformations of the interface, while stability requirements are fulfilled and conservation conditions are respected.

Finally, we illustrate the developed techniques by considering an application with the Euler's equations posed on time-dependent curved multi-domains in two space dimensions. The numerical calculations corroborate stability and accuracy of the fully discrete approximation.

1 INTRODUCTION

Multi-block schemes that use Summation-by-Parts (SBP) operators and the Simultaneous Approximation Terms (SAT) technique [2], have previously been investigated in terms of stability, accuracy and conservation [3, 5, 6, 10, 11]. The focus of the SBP-SAT multi-block methodology has been, so far, mostly on time-independent spatial domains with a notable exception being [13].

In this paper, we extend the multi-block technique for moving domains in [13] and construct an interface formulation that couples two curved domains over a moving and/or deforming interface. The new time-dependent interface formulation is provably stable, accurate and conservative.

The rest of this paper proceeds as follows. In section 2, we transform the continuous problem from Cartesian to curvilinear coordinates and derive a conservative and well-posed interface condition. Section 3 deals with the discrete problem where we guarantee the stability and conservation of the interface procedure. In section 4, numerical experiments are performed and corroborate the results regarding the accuracy, stability and conservation of the scheme. Finally, we summarize and draw conclusions in section 5.

2 THE CONTINUOUS PROBLEM

Consider the following system of equations on a time dependent deforming domain

$$\begin{aligned} U_t + (\hat{A}U)_x + (\hat{B}U)_y = 0,\ (x,\ y) \in \Omega_L(t),\ t \in [0,\ T], \\ V_t + (\hat{A}V)_x + (\hat{B}V)_y = 0,\ (x,\ y) \in \Omega_R(t),\ t \in [0,\ T], \end{aligned} \tag{1}$$

where U, V are the solutions on the left and right sub-domains, the subscripts t, x and y indicate partial derivatives in their respective direction and $\Omega_{L,R}(t)$ are the left and right spatial domains. Moreover, $\hat{A}$ and $\hat{B}$ are constant and symmetric matrices of size l. In (1), $\Omega_{L,R}(t)$ meet at a time-dependent interface denoted by $i(t)$, as shown schematically in Figure 1.

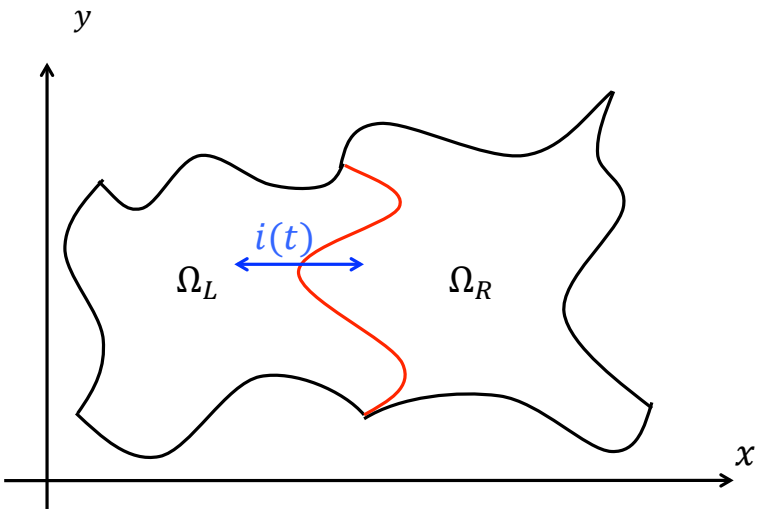

Figure 1: A schematic of the domains $\Omega_{L,R}(t)$ and the time-dependent interface $i(t)$

We transform (1) from the Cartesian coordinates, x and y, into curvilinear coordinates ξ and η by employing a Lagrangian-Eulerian transformation [22]. The dependence between the

coordinates is described by

$$\begin{aligned} x = x(\xi,\ \eta,\ \tau),\ y = y(\xi,\ \eta,\ \tau),\ t = \tau, \\ \xi = \xi(x,\ y,\ t),\ \eta = \eta(x,\ y,\ t),\ \tau = t. \end{aligned} \tag{2}$$

A schematic of the transformed sub-domains, $\Phi_{L,R}$, and the fixed interface between them, i, is shown in Figure 2. For more details about the transformation, see [13].

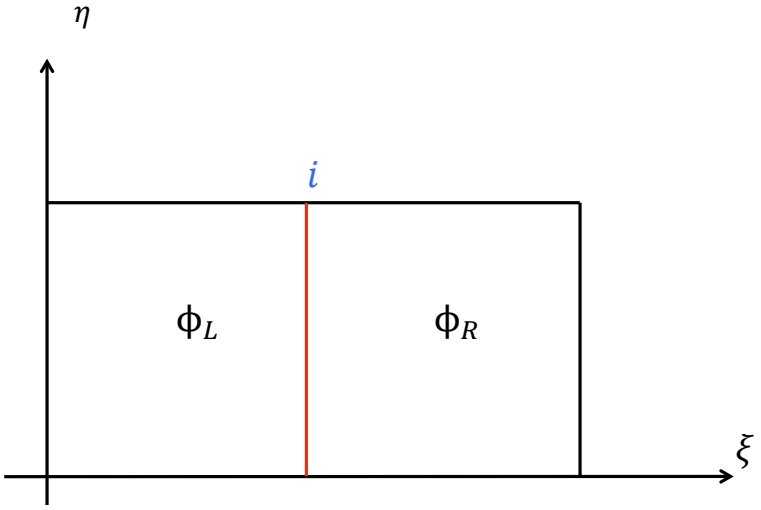

Figure 2: A schematic of the transformed domains $\Phi_{L,R}$ and the time-independent interface i.

The governing equations in (1) are then expressed in terms of ξ and η by using the chain rule, as

$$\begin{aligned} (J_L U_\tau) + (A_L U)_\xi + (B_L U)_\eta = 0,\ (\xi,\ \eta) \in \Phi_L,\ \tau \in [0,\ T], \\ (J_R V_\tau) + (A_R V)_\xi + (B_R V)_\eta = 0,\ (\xi,\ \eta) \in \Phi_R,\ \tau \in [0,\ T], \end{aligned} \tag{3}$$

where $J_{L,R} > 0$ are the determinants of the Jacobian matrix for the left and right transformations, respectively. Moreover,

$$\begin{aligned} A_{L,R} &= (J\xi_t)_{L,R} I + (J\xi_x)_{L,R} \hat{A} + (J\xi_y)_{L,R} \hat{B}, \\ B_{L,R} &= (J\eta_t)_{L,R} I + (J\eta_x)_{L,R} \hat{A} + (J\eta_y)_{L,R} \hat{B}, \end{aligned} \tag{4}$$

where I is the identity matrix of size l. To get the conservative form in (3), we have used the Geometrical Conservation Law (GCL) [12, 13] summarized as $(J_{L_R})_\tau + (A_{L,R})_\xi + (B_{L,R})_\eta = 0$.

2.1 Conservation

To derive conservation conditions, we apply the energy method (multiplying the first and second equations in (3) with ϕ_L^T and ϕ_R^T where $(\phi_{L,R})_j \in H^0$ for $j \in \{1, \dots l\}$ are arbitrary test functions that vanish at the boundaries (not at the interface), and integrate in space and time). The result is

$$\begin{aligned} \int_0^T \iint_{\Phi_L} [(\phi_L^T J_L U)_\tau + (\phi_L^T A_L U)_\xi + (\phi_L^T B_L U)_\eta] d\Phi d\tau = \int_0^T \iint_{\Phi_L} [(\phi_L^T)_\tau J_L U + (\phi_L^T)_\xi A_L U + (\phi_L^T)_\eta B_L U] d\Phi d\tau, \\ \int_0^T \iint_{\Phi_R} [(\phi_R^T J_R V)_\tau + (\phi_R^T A_R V)_\xi + (\phi_R^T B_R V)_\eta] d\Phi d\tau = \int_0^T \iint_{\Phi_R} [(\phi_R^T)_\tau J_R V + (\phi_R^T)_\xi A_R V + (\phi_R^T)_\eta B_R V] d\Phi d\tau. \end{aligned} \tag{5}$$

To derive the total derivatives on the left hand side of both equations in (5), one needs to use the GCL corresponding to the left and right transformations. We add the two relations in (5),

integrate by parts and only consider the terms at the interface. Additionally, at the interface we assume $\phi_L = \phi_R := \phi_i$ to obtain

$$\begin{aligned}\iint_{\Phi_L}(\phi_L^T J_L U)\Big|_{\tau=0}^{\tau=T} d\Phi + \iint_{\Phi_R}(\phi_R^T J_R V)\Big|_{\tau=0}^{\tau=T} d\Phi - \int_0^T \iint_{\Phi_L}\Big[U^T[(J_L\phi_L)_\tau + (A_L\phi_L)_\xi + (B_L\phi_L)_\eta]\Big]^T d\Phi\, d\tau \\ - \int_0^T \iint_{\Phi_R}\Big[V^T[(J_R\phi_R)_\tau + (A_R\phi_R)_\xi + (B_R\phi_R)_\eta]\Big]^T d\Phi\, d\tau \\ = \; - \int_0^T \int_i \underbrace{\phi_i^T(A_{L_i}U_i - A_{R_i}V_i)}_{IT} d\eta\, d\tau\end{aligned} \tag{6}$$

where the subscript i denotes interface and IT indicates interface term. To derive the IT, we have used the Green-Gauss theorem. Moreover, we have again applied the GCL in order to arrive at the weak forms on the left hand side of (6). Further, we note that the following terms are included in IT

$$\begin{aligned}A_{L_i} &= (J\xi_t)_L I + (J\xi_x)_L \hat{A} + (J\xi_y)_L \hat{B}, \\ A_{R_i} &= (J\xi_t)_R I + (J\xi_x)_R \hat{A} + (J\xi_y)_R \hat{B},\end{aligned} \tag{7}$$

where the following relations between the metric terms and their counterparts corresponding to the inverse transformation hold

$$(J\xi_t)_{L,R} = (x_\eta y_\tau - x_\tau y_\eta)_{L,R}, \;\; (J\xi_x)_{L,R} = (y_\eta)_{L,R}, \;\; (J\xi_y)_{L,R} = (-x_\eta)_{L,R}. \tag{8}$$

The two domains, $\Omega_{L,R}(t)$, are always connected at the interface regardless of the movements and deformations. Therefore, the left and right transformations map the same curve ($i(t)$ in the Cartesian coordinates) to the same line segment (i in the curvilinear coordinates). Hence, although the left and right transformations may differ in general, the left and right metrics terms in (8) will have exactly the same values at the interface. We conclude that

$$A_{L_i} = A_{R_i} := A_i \tag{9}$$

and $U_i = V_i$ removes the interface term. Finally, (6) becomes an integral statement of the original problem and conservation is respected. Condition (9) will need to be respected also in the numerical approximations as we will show below.

2.2 Well-posedness

The energy method (multiplying (3) with the transpose of the solution and integrating over the spatial and temporal domains) together with the Green-Gauss theorem results in

$$\begin{aligned}||U(T,\,\xi,\,\eta)||_{J_L}^2 &= ||U(0,\,\xi,\,\eta))||_{J_L}^2 - \int_0^T \oint_{\delta\Phi_L} U^T C_L\, U\; ds\; d\tau, \\ ||V(T,\,\xi,\,\eta)||_{J_R}^2 &= ||V(0,\,\xi,\,\eta))||_{J_R}^2 - \int_0^T \oint_{\delta\Phi_R} V^T C_R\, V\; ds\; d\tau.\end{aligned} \tag{10}$$

In (10), the norm is defined as $||W||_{J_{L,R}}^2 = \iint_{\Phi_{L,R}} W^T J_{L,R} W\; d\xi\; d\eta$, for $W \in \{U, V\}$ and $\delta\Phi_{L,R}$ are the boundaries of $\Phi_{L,R}$. Moreover, $C_{L,R} = (A_{L,R},\; B_{L,R}) \cdot n_{L,R}$ where $n_{L,R} = (\alpha_{L,R},\; \beta_{L,R})$

is the outward pointing normal vector from $\Phi_{L,R}$. Further, $C_{L,R}$ can be expanded as $C_{L,R} = \alpha_{L,R}A_{L,R} + \beta_{L,R}B_{L,R}$ and due to symmetry be decomposed into $C_{L,R} = X_{L,R}\Lambda_{L,R}X_{L,R}^T$ where $\Lambda_{L,R}$ is the matrix of eigenvalues of $C_{L,R}$ and $X_{L,R}$ is the corresponding eigenvector matrix.

To control the growth of the energy of the solution due to boundary terms, we choose the following far-field well-posed boundary conditions

$$\begin{array}{l}(X_L^T U)_j = (X_L^T U_\infty)_j \ \text{ if } \ (\Lambda_L)_{jj} < 0, \\ (X_R^T V)_j = (X_R^T V_\infty)_j \ \text{ if } \ (\Lambda_R)_{jj} < 0,\end{array} \tag{11}$$

where U_∞, V_∞ are the data to the problem and $j \in \{1, \ldots, l\}$. Additionally, at the interface where $n_L = (1,\ 0)^T$ and $n_R = (-1,\ 0)^T$, we have $C_L = A_i$ and $C_R = -A_i$ and the decomposition $A_i = X_i\Lambda_i X_i^T$.

By substituting (11) in (10), observing that $U_i = V_i$, and considering the initial conditions $U(0,\ \xi,\ \eta) = f_L$ and $V(0,\ \xi,\ \eta) = f_R$, we find

$$\begin{aligned}||U(T,\xi,\eta)||_{J_L}^2 + ||V(T,\xi,\eta)||_{J_R}^2 \ &= \ ||f_L||_{J_L}^2 + ||f_R||_{J_R}^2 \\ &- \int_0^T\!\!\int_{\delta\Phi_L\setminus i} \left[(X_L^T U)^T\Lambda_L^+(X_L^T U) - (X_L^T U_\infty)^T\Lambda_L^-(X_L^T U_\infty)\right] ds\, d\tau \\ &- \int_0^T\!\!\int_{\delta\Phi_R\setminus i} \left[(X_R^T V)^T\Lambda_R^+(X_R^T V) - (X_R^T V_\infty)^T\Lambda_R^-(X_R^T V_\infty)\right] ds\, d\tau,\end{aligned} \tag{12}$$

where the positive and negative superscripts in $\Lambda_L^{+,-}$, $\Lambda_R^{+,-}$ and $\Lambda_i^{+,-}$ restrict $\Lambda_{L,R,i}$ to the non-negative and negative eigenvalues, respectively. Finally, we conclude that the energy of the solution is bounded by data and that the problem is strongly well-posed [21].

3 THE DISCRETE PROBLEM

We discretize the left and right sub-domains using $N_{L,R}$ and M grid points in the ξ and η directions, respectively. In this article, we consider matching grid points along the interface. For non-conforming grids at the interface, interpolation techniques must be used [24, 25] in order to couple the blocks. However, with the added difficulty of a moving interface we refrain from this technical complication and will consider that in a future paper. We use K time levels from 0 to T and tensor products to arrange the fully discrete numerical solution. As an example, the numerical solution on the left sub-domain is arranged as

$$\mathbf{U} = \begin{bmatrix} \mathbf{U}_1 \\ \vdots \\ [\mathbf{U}_k] \\ \vdots \\ \mathbf{U}_K \end{bmatrix};\ [\mathbf{U}_k] = \begin{bmatrix} \mathbf{U}_1 \\ \vdots \\ [\mathbf{U}_i] \\ \vdots \\ \mathbf{U}_{N_L} \end{bmatrix}_k;\ [\mathbf{U}_i]_k = \begin{bmatrix} \mathbf{U}_1 \\ \vdots \\ \mathbf{U}_j \\ \vdots \\ \mathbf{U}_M \end{bmatrix}_{ki}, \tag{13}$$

in which $\mathbf{U}_{kij} \approx U(\tau_k,\ \xi_i,\ \eta_j)$ for $(\xi,\ \eta) \in \Phi_L$. The fully discrete numerical solution corresponding to the right sub-domain is denoted by $\mathbf{V}$ and arranged in the same way.

The first derivative u_ξ is approximated by $D_\xi\mathbf{u}$, where D_ξ is a so-called SBP operator of the form

$$D_\xi = P_\xi^{-1}Q_\xi, \tag{14}$$

and $\mathbf{u} = [u_0,\ u_1,\ \cdots,\ u_N]^T$ is the solution vector evaluated in each grid point in the ξ direction. P_ξ is a symmetric positive definite matrix, and Q_ξ is an almost skew-symmetric matrix that satisfies

$$Q_\xi + Q_\xi^T = E_1 - E_0 = B = diag(-1, 0, ..., 0, 1). \tag{15}$$

In (15), $E_0 = diag(1, 0, ..., 0)$ and $E_1 = diag(0, ..., 0, 1)$. The η and τ directions are discretized in the same way.

A first derivative SBP operator is a 2s-order accurate central difference operator which is modified close to the boundaries such that it becomes one-sided. Together with a diagonal norm P, the boundary closure is s-order accurate, making a stable first order approximation of a hyperbolic problem s+1 order accurate globally [4, 9]. For more details on non-standard SBP operators see [15, 18, 16, 17].

A finite difference approximation including the time discretization [7, 8], on SBP-SAT form, is constructed by extending the one-dimensional SBP operators in a tensor product fashion as

$$\begin{aligned} D_\tau &= P_\tau^{-1} Q_\tau \otimes I_\xi \otimes I_\eta \otimes I, \\ D_\xi &= I_\tau \otimes P_\xi^{-1} Q_\xi \otimes I_\eta \otimes I, \\ D_\eta &= I_\tau \otimes I_\xi \otimes P_\eta^{-1} Q_\eta \otimes I, \end{aligned} \tag{16}$$

where $\otimes$ represents the Kronecker product [14]. Here and in the remainder of this article, all matrices in the first position are of size $K \times K$, the second position $N_{L,R} \times N_{L,R}$, the third position $M \times M$ and the fourth position $l \times l$. Additionally, the identity matrix, I, has a consistent size with its position in the Kronecker product.

Prior to discretizing (3), we use the splitting technique explained in [19]. The discrete version of (3) including only the interface term (the far-field boundaries are addressed in [13] and are not repeated here) is

$$\begin{aligned} &\frac{1}{2}[D_\tau \mathbf{J}_L \mathbf{U} + \mathbf{J}_L D_\tau \mathbf{U} + (\mathbf{J}_L)_\tau \mathbf{U} + D_\xi \mathbf{A}_L \mathbf{U} + \mathbf{A}_L D_\xi \mathbf{U} + (\mathbf{A}_L)_\xi \mathbf{U} + D_\eta \mathbf{B}_L \mathbf{U} + \mathbf{B}_L D_\eta \mathbf{U} + (\mathbf{B}_L)_\eta \mathbf{U}] = \\ &\qquad (I_\tau \otimes P_\xi^{-1} E_1 \otimes I_\eta \otimes I) \Sigma_L (\mathbf{U} - \mathbf{V}) \\ &\frac{1}{2}[D_\tau \mathbf{J}_R \mathbf{V} + \mathbf{J}_R D_\tau \mathbf{V} + (\mathbf{J}_R)_\tau \mathbf{V} + D_\xi \mathbf{A}_R \mathbf{V} + \mathbf{A}_R D_\xi \mathbf{V} + (\mathbf{A}_R)_\xi \mathbf{V} + D_\eta \mathbf{B}_R \mathbf{V} + \mathbf{B}_R D_\eta \mathbf{V} + (\mathbf{B}_R)_\eta \mathbf{V}] = \\ &\qquad (I_\tau \otimes P_\xi^{-1} E_0 \otimes I_\eta \otimes I) \Sigma_R (\mathbf{V} - \mathbf{U}), \end{aligned} \tag{17}$$

where $\Sigma_{L,R}$ are matrices of size $(KNMl) \times (KNMl)$ and operate as penalty parameters corresponding to the weak interface treatments for the left and right sub-domains, respectively, and will be chosen later based on conservation and stability requirements. Moreover, $\mathbf{J}_{L,R}, \mathbf{A}_{L,R}, \mathbf{B}_{L,R}, (\mathbf{A}_{L,R})_\xi$ and $(\mathbf{B}_{L,R})_\eta$ are block diagonal matrices of size $(KN_{L,R}Ml) \times (KN_{L,R}Ml)$, where each $l \times l$ block approximates respectively $J_{L,R}, A_{L,R}, B_{L,R}, (A_{L,R})_\xi$ and $(B_{L,R})_\eta$ on a grid point. Note that the SBP operators are not necessarily the same on the left and right sub-domains. To ease the notation the subscripts L, R on the derivatives $D_{\xi,\eta,\tau}$ are dropped.

3.1 Conservation

To show that the scheme is conservative, we multiply (17) by arbitrary vector functions $\phi_L^T P$ and $\phi_R^T P$, where $P = (P_\tau \otimes P_\xi \otimes P_\eta \otimes I)$. Moreover, we use the SBP property stated in (15)

and focus on the interface to obtain

$$\begin{aligned}
&\phi_L^T[(E_1-E_0)\otimes P_\xi\otimes P_\eta\otimes I]\mathbf{J}_L\mathbf{U}+\phi_L^T(P_\tau\otimes E_1\otimes P_\eta\otimes I)\mathbf{A}_L\mathbf{U}\\
&-\frac{1}{2}\Big[\mathbf{U}^TP[D_\tau\mathbf{J}_L\phi_L+\mathbf{J}_LD_\tau\phi_L+(\mathbf{J}_L)_\tau\phi_L]\Big]^T-\frac{1}{2}\Big[\mathbf{U}^TP[D_\xi\mathbf{A}_L\phi_L+\mathbf{A}_LD_\xi\phi_L+(\mathbf{A}_L)_\xi\phi_L]\Big]^T\\
&-\frac{1}{2}\Big[\mathbf{U}^TP[D_\eta\mathbf{B}_L\phi_L+\mathbf{B}_LD_\eta\phi_L+(\mathbf{B}_L)_\eta\phi_L]\Big]^T=\phi_L^T(P_\tau\otimes E_1\otimes P_\eta\otimes I)\Sigma_L(\mathbf{U}-\mathbf{V})\\
&\phi_R^T[(E_1-E_0)\otimes P_\xi\otimes P_\eta\otimes I]\mathbf{J}_R\mathbf{V}-\phi_R^T(P_\tau\otimes E_0\otimes P_\eta\otimes I)\mathbf{A}_R\mathbf{V}\\
&-\frac{1}{2}\Big[\mathbf{V}^TP[D_\tau\mathbf{J}_R\phi_R+\mathbf{J}_RD_\tau\phi_R+(\mathbf{J}_R)_\tau\phi_R]\Big]^T-\frac{1}{2}\Big[\mathbf{V}^TP[D_\xi\mathbf{A}_R\phi_R+\mathbf{A}_RD_\xi\phi_R+(\mathbf{A}_R)_\xi\phi_R]\Big]^T\\
&-\frac{1}{2}\Big[\mathbf{V}^TP[D_\eta\mathbf{B}_R\phi_R+\mathbf{B}_RD_\eta\phi_R+(\mathbf{B}_R)_\eta\phi_R]\Big]^T=\phi_R^T(P_\tau\otimes E_0\otimes P_\eta\otimes I)\Sigma_R(\mathbf{V}-\mathbf{U}).
\end{aligned}\tag{18}$$

In order to arrive at (18), we have used the symmetry property of the matrices as well as the Numerical Geometric Conservation Law (NGCL) summarized as $(\mathbf{J}_\tau)_{L,R}+(\mathbf{A}_\xi)_{L,R}+(\mathbf{B}_\eta)_{L,R}=0$. For more details on NGCL see [13]. Now, we consider the same $P_{\eta,\tau}$ in the left and right subdomains and add the two relations in (18). The result is

$$\begin{aligned}
&\phi_L^T[(E_1-E_0)\otimes P_\xi\otimes P_\eta\otimes I]\mathbf{J}_L\mathbf{U}+\phi_R^T[(E_1-E_0)\otimes P_\xi\otimes P_\eta\otimes I]\mathbf{J}_R\mathbf{V}\\
&-\frac{1}{2}\Big[\mathbf{U}^TP[(D_\tau\mathbf{J}_L\phi_L+\mathbf{J}_LD_\tau\phi_L+(\mathbf{J}_L)_\tau\phi_L)\Big]^T-\frac{1}{2}\Big[\mathbf{U}^TP[D_\xi\mathbf{A}_L\phi_L+\mathbf{A}_LD_\xi\phi_L+(\mathbf{A}_L)_\xi\phi_L]\Big]^T\\
&-\frac{1}{2}\Big[\mathbf{U}^TP[D_\eta\mathbf{B}_L\phi_L+\mathbf{B}_LD_\eta\phi_L+(\mathbf{B}_L)_\eta\phi_L]\Big]^T-\frac{1}{2}\Big[\mathbf{V}^TP[D_\tau\mathbf{J}_R\phi_R+\mathbf{J}_RD_\tau\phi_R+(\mathbf{J}_R)_\tau\phi_R]\Big]^T\\
&-\frac{1}{2}\Big[\mathbf{V}^TP[D_\xi\mathbf{A}_R\phi_R+\mathbf{A}_RD_\xi\phi_R+(\mathbf{A}_R)_\xi\phi_R]\Big]^T-\frac{1}{2}\Big[\mathbf{V}^TP[D_\eta\mathbf{B}_R\phi_R+\mathbf{B}_RD_\eta\phi_R+(\mathbf{B}_R)_\eta\phi_R]\Big]^T\\
&=-\phi_L^T(P_\tau\otimes E_1\otimes P_\eta\otimes I)\mathbf{A}_L\mathbf{U}+\phi_L^T(P_\tau\otimes E_1\otimes P_\eta\otimes I)\Sigma_L(\mathbf{U}-\mathbf{V})\\
&+\phi_R^T(P_\tau\otimes E_0\otimes P_\eta\otimes I)\mathbf{A}_R\mathbf{V}+\phi_R^T(P_\tau\otimes E_0\otimes P_\eta\otimes I)\Sigma_R(\mathbf{V}-\mathbf{U}).
\end{aligned}\tag{19}$$

As in the continuous problem, $\phi_L=\phi_R:=\phi_i$ at the interface, by which the right hand side of (19) becomes

$$\phi_i^T(P_\tau\otimes P_\eta\otimes I)[-\mathbf{A}_{L_i}\mathbf{U}_i+\mathbf{A}_{R_i}\mathbf{V}_i+(\Sigma_{L_i}-\Sigma_{R_i})(\mathbf{U}_i-\mathbf{V}_i)],\tag{20}$$

where the subscript i restricts the vectors and matrices to the interface, i.e. $\mathbf{U}_i$ is now of size KMl. Since $\mathbf{A}_L$ and $\mathbf{A}_R$ include pointwise approximations to A_L and A_R in (7), respectively, we have

$$\begin{aligned}
\mathbf{A}_L&=(\overline{J\xi_t})_L(I_\tau\otimes I_\xi\otimes I_\eta\otimes I)+(\overline{J\xi_x})_L(I_\tau\otimes I_\xi\otimes I_\eta\otimes\hat{A})+(\overline{J\xi_y})_L(I_\tau\otimes I_\xi\otimes I_\eta\otimes\hat{B}),\\
\mathbf{A}_R&=(\overline{J\xi_t})_R(I_\tau\otimes I_\xi\otimes I_\eta\otimes I)+(\overline{J\xi_x})_R(I_\tau\otimes I_\xi\otimes I_\eta\otimes\hat{A})+(\overline{J\xi_y})_R(I_\tau\otimes I_\xi\otimes I_\eta\otimes\hat{B}),
\end{aligned}\tag{21}$$

where the bar sign is used to indicate that the metric terms are approximated numerically. The numerical metric terms are evaluated as

$$\overline{J\xi_t}=diag[D_\eta(D_\eta M^{(1)}-D_\xi M^{(2)})],\ \ \overline{J\xi_x}=diag[D_\eta\mathbf{y}],\ \ \overline{J\xi_y}=-diag[D_\eta\mathbf{x}],\tag{22}$$

where **x, y** are the x and y coordinates of the mesh in the Cartesian coordinate system, arranged in a vector, consistent to (13). Moreover, $M^{(1)}=diag(\mathbf{y})D_\xi\mathbf{x}$ and $M^{(2)}=diag(\mathbf{y})(D_\eta\mathbf{x})$. To see more details about the numerical metrics, see [13, 23]. From (21) and (22) one can conclude that if we have matching grid points along the interface, and use the same SBP operators for

the left and right problems, we have $\mathbf{A}_{L_i} = \mathbf{A}_{R_i} := \mathbf{A_i}$, which correspond to the continuous requirement in (9).

We use the decomposition $\mathbf{A}_i = \mathbf{X}_i\mathbf{\Lambda}_i\mathbf{X}_i^T$ and choose $\Sigma_{L_i,R_i} = \mathbf{X}_i\tilde{\Sigma}_{L_i,R_i}\mathbf{X}_i^T$ where $\tilde{\Sigma}_{L_i,R_i}$ are diagonal and rewrite (20) as

$$\phi_i^T(P_\tau \otimes P_\eta \otimes I)\left[\mathbf{X}_i(-\mathbf{\Lambda}_i + \tilde{\Sigma}_{L_i} - \tilde{\Sigma}_{R_i})\mathbf{X}_i^T\right](\mathbf{U}_i - \mathbf{V}_i). \tag{23}$$

In order to obtain a conservative scheme, $\tilde{\Sigma}_{L_i,R_i}$ must be chosen such that

$$-\mathbf{\Lambda}_i + \tilde{\Sigma}_{L_i} - \tilde{\Sigma}_{R_i} = 0 \tag{24}$$

holds.

3.2 Stability

To prove stability we apply the discrete energy method (multiplying the left and right sub-problems with $\mathbf{U}^T P$ and $\mathbf{V}^T P$, respectively) on (17). We add the transpose of the result to itself and use the SBP property (15) to arrive at

$$\begin{aligned}
&\mathbf{U}^T[(E_1 - E_0) \otimes P_\xi \otimes P_\eta \otimes I]\mathbf{J}_L\mathbf{U} + \mathbf{U}^T[P_\tau \otimes (E_1 - E_0) \otimes P_\eta \otimes I]\mathbf{A}_L\mathbf{U} + \\
&\mathbf{U}^T[P_\tau \otimes P_\xi \otimes (E_1 - E_0) \otimes I]\mathbf{B}_L\mathbf{U} = \mathbf{U}^T(P_\tau \otimes E_1 \otimes P_\eta \otimes I)\Sigma_L(\mathbf{U} - \mathbf{V}) + \\
&(\mathbf{U} - \mathbf{V})^T\Sigma_L^T(P_\tau \otimes E_1 \otimes P_\eta \otimes I)\mathbf{U}, \\
&\mathbf{V}^T[(E_1 - E_0) \otimes P_\xi \otimes P_\eta \otimes I]\mathbf{J}_R\mathbf{V} + \mathbf{V}^T[P_\tau \otimes (E_1 - E_0) \otimes P_\eta \otimes I]\mathbf{A}_R\mathbf{V} + \\
&\mathbf{V}^T[P_\tau \otimes P_\xi \otimes (E_1 - E_0) \otimes I]B_R\mathbf{V} = \mathbf{V}^T(P_\tau \otimes E_0 \otimes P_\eta \otimes I)\Sigma_R(\mathbf{V} - \mathbf{U}) + \\
&(\mathbf{V} - \mathbf{U})^T\Sigma_R^T(P_\tau \otimes E_0 \otimes P_\eta \otimes I)\mathbf{V}.
\end{aligned} \tag{25}$$

Again, we have used the NGCL in order to obtain (25). We simplify (25) and only keep the terms at the interface which gives

$$\begin{aligned}
&||\mathbf{U}_K||^2_{(P_\xi \otimes P_\eta \otimes I)\mathbf{J}_{L_K}} - ||\mathbf{U}_1||^2_{(P_\xi \otimes P_\eta \otimes I)\mathbf{J}_{L_1}} = \mathbf{U}^T[P_\tau \otimes -E_1 \otimes P_\eta \otimes I]\mathbf{A}_L\mathbf{U} + \\
&\mathbf{U}^T(P_\tau \otimes E_1 \otimes P_\eta \otimes I)\Sigma_L(\mathbf{U} - \mathbf{V}) + (\mathbf{U} - \mathbf{V})^T\Sigma_L^T(P_\tau \otimes E_1 \otimes P_\eta \otimes I)\mathbf{U} \\
&||\mathbf{V}_K||^2_{(P_\xi \otimes P_\eta \otimes I)\mathbf{J}_{R_K}} - ||\mathbf{V}_1||^2_{(P_\xi \otimes P_\eta \otimes I)\mathbf{J}_{R_1}} = \mathbf{V}^T[P_\tau \otimes E_0 \otimes P_\eta \otimes I]\mathbf{A}_R\mathbf{V} + \\
&\mathbf{V}^T(P_\tau \otimes E_0 \otimes P_\eta \otimes I)\Sigma_R(\mathbf{V} - \mathbf{U}) + (\mathbf{V} - \mathbf{U})^T\Sigma_R^T(P_\tau \otimes E_0 \otimes P_\eta \otimes I)\mathbf{V}.
\end{aligned} \tag{26}$$

The norms in (26) are given by $||\mathbf{W}||^2_{H_{L,R}} = \mathbf{W}^T H_{L,R}\mathbf{W}$, where $H_{L,R} = (P_\xi \otimes P_\eta \otimes I)\mathbf{J}_{L,R} > 0$ for $\mathbf{W} \in \{\mathbf{U},\ \mathbf{V}\}$. Moreover, the subscripts K and 1 indicate restrictions to the last and first time levels, respectively. We add the two relations in (26) and again use the decompositions $\mathbf{A}_i = \mathbf{X}_i\mathbf{\Lambda}_i\mathbf{X}_i^T$ and $\Sigma_{L_i,R_i} = \mathbf{X}_i\tilde{\Sigma}_{L_i,R_i}\mathbf{X}_i^T$ to obtain

$$\begin{aligned}
&||\mathbf{U}_K||^2_{(P_\xi \otimes P_\eta \otimes I)\mathbf{J}_{L_K}} + ||\mathbf{V}_K||^2_{(P_\xi \otimes P_\eta \otimes I)\mathbf{J}_{R_K}} = ||\mathbf{U}_1||^2_{(P_\xi \otimes P_\eta \otimes I)\mathbf{J}_{L_1}} + ||\mathbf{V}_1||^2_{(P_\xi \otimes P_\eta \otimes I)\mathbf{J}_{R_1}} + \\
&\begin{bmatrix} \mathbf{X}_i^T\mathbf{U}_i \\ \mathbf{X}_i^T\mathbf{V}_i \end{bmatrix}^T \left[P_\tau \otimes P_\eta \otimes I \otimes \tilde{I}_1\right] \begin{bmatrix} -\mathbf{\Lambda}_i + 2\tilde{\Sigma}_{L_i} & -(\tilde{\Sigma}_{L_i} + \tilde{\Sigma}_{R_i}) \\ -(\tilde{\Sigma}_{L_i} + \tilde{\Sigma}_{R_i}) & \mathbf{\Lambda}_i + 2\tilde{\Sigma}_R \end{bmatrix} \begin{bmatrix} \mathbf{X}_i^T\mathbf{U}_i \\ \mathbf{X}_i^T\mathbf{V}_i \end{bmatrix},
\end{aligned} \tag{27}$$

where $\tilde{I}$ is

$$\tilde{I}_1 = \begin{bmatrix} 1 & 1 \\ 1 & 1 \end{bmatrix}. \tag{28}$$

By considering the conservation requirement on the penalty operators in (24), (27) becomes

$$||\mathbf{U}_K||^2_{(P_\xi\otimes P_\eta\otimes I)\mathbf{J}_{L_K}} + ||\mathbf{V}_K||^2_{(P_\xi\otimes P_\eta\otimes I)\mathbf{J}_{R_K}} = ||\mathbf{U}_1||^2_{(P_\xi\otimes P_\eta\otimes I)\mathbf{J}_{L_1}} + ||\mathbf{V}_1||^2_{(P_\xi\otimes P_\eta\otimes I)\mathbf{J}_{R_1}} + \\ \left[\ \mathbf{X}_i^T(\mathbf{U}_i-\mathbf{V}_i)\ \right]^T (P_\tau\otimes P_\eta\otimes I)\left[-\mathbf{\Lambda}_i + 2\tilde{\Sigma}_{L_i}\right]\ \mathbf{X}_i^T(\mathbf{U}_i-\mathbf{V}_i). \tag{29}$$

From (29), we conclude that the following conditions lead to a stable interface treatment

$$\begin{array}{lcll} (\tilde{\Sigma}_{L_i})_{jj} & \leq & (\mathbf{\Lambda}_i)_{jj}/2 & \text{if} \quad (\mathbf{\Lambda}_i)_{jj} < 0, \\ (\tilde{\Sigma}_{L_i})_{jj} & = & 0 & \text{if} \quad (\mathbf{\Lambda}_i)_{jj} \geq 0, \end{array} \tag{30}$$

for $j \in \{1,\ldots,l\}$. As an example if we let $\tilde{\Sigma}_{L_i} = \mathbf{\Lambda}_i^-$, where the negative superscription restricts $\mathbf{\Lambda}_i$ to the negative eigenvalues. Then (29) becomes

$$||\mathbf{U}_K||^2_{(P_\xi\otimes P_\eta\otimes I)\mathbf{J}_{L_K}} + ||\mathbf{V}_K||^2_{(P_\xi\otimes P_\eta\otimes I)\mathbf{J}_{R_K}} = ||\mathbf{U}_1||^2_{(P_\xi\otimes P_\eta\otimes I)\mathbf{J}_{L_1}} + ||\mathbf{V}_1||^2_{(P_\xi\otimes P_\eta\otimes I)\mathbf{J}_{R_1}} - \\ (\mathbf{U}_i-\mathbf{V}_i)^T\ (P_\tau\otimes P_\eta\otimes I)\underbrace{|\mathbf{X}_i\mathbf{\Lambda}_i\mathbf{X}_i^T|}_{=|\mathbf{A}_i|}\ (\mathbf{U}_i-\mathbf{V}_i) \tag{31}$$

which represents a dissipative, stable and conservative interface procedure.

4 NUMERICAL EXPERIMENTS

We consider the two-dimensional constant coefficient symmetrized Euler equations [20] described by

$$W_t + \hat{A}W_x + \hat{B}W_y = 0,\ (x,\ y) \in \Omega_{L,R}(t),\ t \in [0,\ T], \tag{32}$$

where

$$W = \left[\frac{\bar{c}\rho}{\sqrt{\gamma}\bar{\rho}},\ u,\ v,\ \frac{\theta}{\bar{c}\sqrt{\gamma(\gamma-1)}}\right]^T. \tag{33}$$

In (33), $W \in \{U,\ V\}$, and $\rho,\ u,\ v,\ \theta,$ and γ are respectively the density, the x and y velocity components, the temperature and the ratio of specific heats. An equation of state of the form $\gamma p = \bar{\rho}\theta + \rho\bar{\theta}$, where p is the pressure, completes the system (32). Moreover, the bar sign denotes the reference state around which we have linearized. The matrices in (32) are

$$\hat{A} = \begin{bmatrix} \bar{u} & \bar{c}/\sqrt{\gamma} & 0 & 0 \\ \bar{c}/\sqrt{\gamma} & \bar{u} & 0 & \sqrt{\frac{\gamma-1}{\gamma}}\bar{c} \\ 0 & 0 & \bar{u} & 0 \\ 0 & \sqrt{\frac{\gamma-1}{\gamma}}\bar{c} & 0 & \bar{u} \end{bmatrix},\ \hat{B} = \begin{bmatrix} \bar{v} & 0 & \bar{c}/\sqrt{\gamma} & 0 \\ 0 & \bar{v} & 0 & 0 \\ \bar{c}/\sqrt{\gamma} & 0 & \bar{v} & \sqrt{\frac{\gamma-1}{\gamma}}\bar{c} \\ 0 & 0 & \sqrt{\frac{\gamma-1}{\gamma}}\bar{c} & \bar{v} \end{bmatrix}. \tag{34}$$

We prescribe $\gamma = 1.4$, $\bar{c} = 2$, $\bar{\rho} = 1$ and consider a mean velocity field of the form $(\bar{u},\ \bar{v}) = (1,\ 1)$. The geometries $\Omega_{L,R}(t)$ are described by

$$\Omega_L(t): \begin{cases} x_{w_L}(y) & = -1 - 0.1\ \sin(2\pi y), \\ x_i(t,\ y) & = -0.1\ [\sin(\pi t) + \cos(2\pi t)\sin(2\pi y)], \\ y_{s_L}(t,\ x) & = -0.05\ \sin[2\pi(x_i(t)-x)/(x_i(t)+1)], \\ y_{n_L}(t,\ x) & = 1 - 0.05\ \sin[2\pi(x_i(t)-x)/(x_i(t)+1)], \end{cases} \tag{35}$$

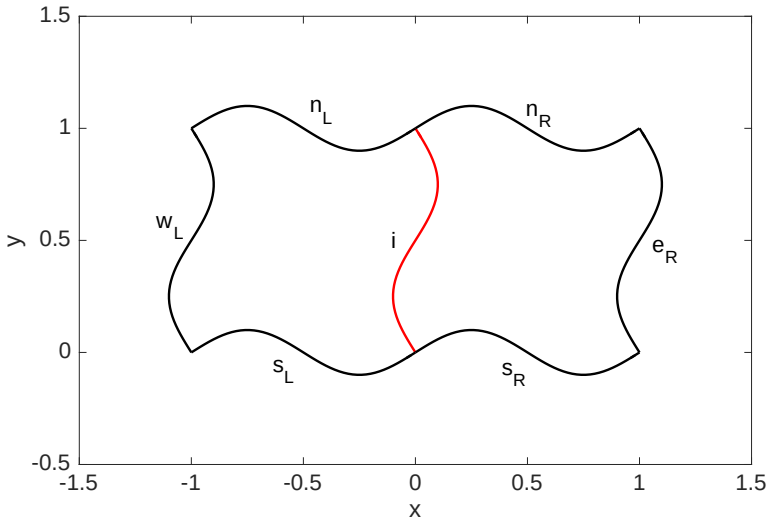

Figure 3: A schematic of $\Omega_{L,R}$ and the boundaries

and

$$\Omega_R(t): \begin{cases} x_{e_R}(y) &= 1 - 0.1\ \sin(2\pi y), \\ x_i(t,\ y) &= -0.1\ [\sin(\pi t) + \cos(2\pi t)\sin(2\pi y)], \\ y_{s_R}(t,x) &= -0.05\ \sin[2\pi(x - x_i(t))/(1 - x_i(t))], \\ x_{n_R}(t,y) &= 1 + 0.05\ \sin[2\pi(x - x_i(t))/(1 - x_i(t))], \end{cases} \tag{36}$$

where $w_L,\ e_R,\ s_{L,R},\ n_{L,R}$ and i are schematically defined in Figure 3.

As seen in (35) and (36), also the four adjacent boundaries $n_{L,R}, s_{L_R}$ to the interface are slightly deforming. To see the details of how to treat deforming boundaries, see [13].

4.1 Accuracy

To conclude the accuracy of our numerical approximations, we use the method of manufactured solution with the reference solution W_∞

$$W_\infty = [5\sin(x-t),\ 5\cos(x-t),\ 10\sin(y-t),\ 10\cos(y-t)]^T \tag{37}$$

which is injected as a forcing function to the right hand side of (32). Moreover, characteristic boundary conditions [13] are used.

We examine the scheme for SBP operators of order $2s$ in the interior and s close to the boundaries in space, where $s \in \{1,\ 2,\ 3\}$. The fifth order accurate SBP operator i.e. SBP84, with a sufficiently large K, is used in time. The rates of convergence are calculated and shown in tables 1-3.

$N_{L,R}, M$	21	31	41
ρ	2.40229	2.08909	2.03912
u	2.13136	2.03877	2.01409
v	2.06440	2.03268	2.01787
p	2.48489	2.12153	2.04978

Table 1: Convergence rates at T=1, for a sequence of mesh refinements, SBP21 in space, SBP84 in time (K=201)

The convergence results in tables 1-3 are correct according to the theory [4, 2].

$N_{L,R}, M$	21	31	41
ρ	3.08961	2.94594	2.93760
u	3.22104	3.11838	3.06405
v	2.91411	2.99215	3.02028
p	3.16628	3.12290	3.08363

Table 2: Convergence rates at T=1, for a sequence of mesh refinements, SBP42 in space, SBP84 in time (K=201)

$N_{L,R}, M$	21	31	41
ρ	4.68075	4.45144	4.60620
u	3.87224	4.15980	4.48346
v	3.84525	3.94578	4.28970
p	3.73903	4.50886	4.75789

Table 3: Convergence rates at T=1, for a sequence of mesh refinements, SBP63 in space, SBP84 in time (K=201)

4.2 An application

We consider an initial pressure of the form $p = e^{-20((x+1)^2+y^2)}$ together with zero velocities and densities everywhere in the left and right sub-domains. Characteristic boundary conditions with data from manufactured solution $p_\infty = e^{-20((x+1-2t)^2+(y-t)^2)}$ is used for far-field boundaries. Moreover, we construct a grid of 41×41 points in space and 81 nodes in time. Third and fifth order accurate SBP operators in space and time, respectively, are used.

The pressure distribution at different times (the red and/or dashed curves corresponding to $\Omega_{L,R}(0)$) are shown in Figures 4-11. As shown in the figures, the pressure pulse passes across the interface smoothly and moves out of the domain as time passes.

5 SUMMARY AND CONCLUSIONS

We have constructed a numerical scheme that satisfies the summation-by-parts convention in combination with the simultaneous approximation term technique, for general multi-block problems with time-dependent deforming interfaces in several space dimensions.

We have studied well-posedness, stability and as well continuous and discrete conservation by employing the continuous and discrete versions of the energy method as our analytical tools and constructed a dissipative, conservative and stable scheme.

An application using the Euler equations posed on a time-dependent multi-block geometry with a moving and deforming interface, was presented. The correct rates of convergence toward the exact solution, were concluded.

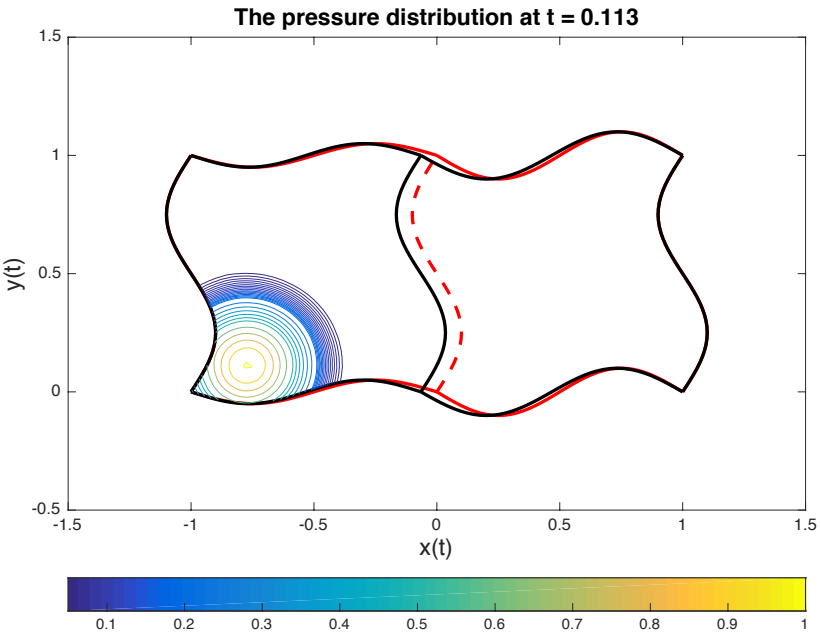

Figure 4: The pressure distribution.

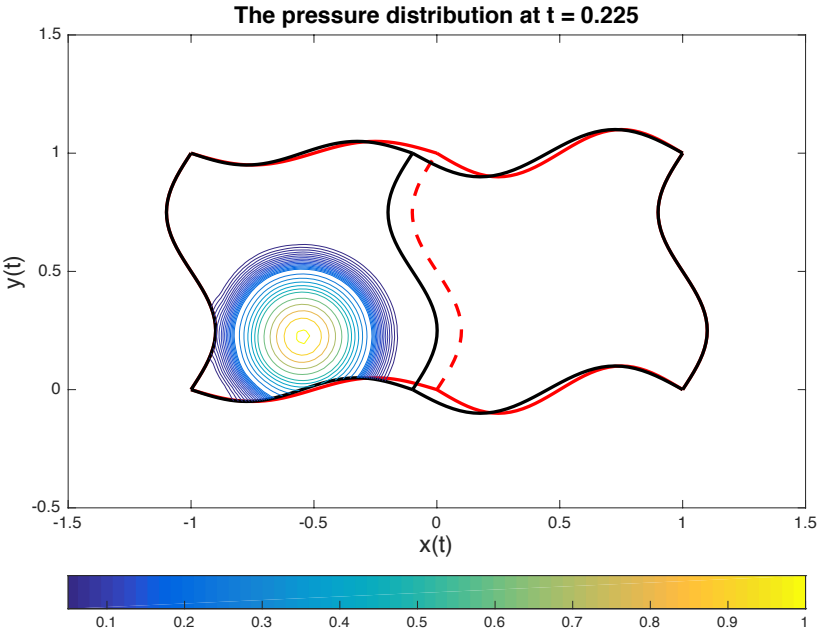

Figure 5: The pressure distribution.

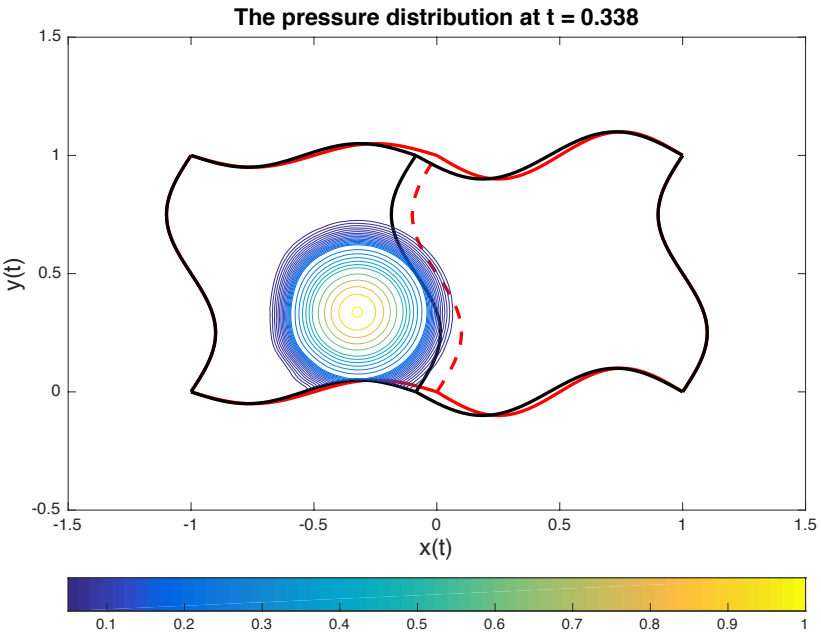

Figure 6: The pressure distribution.

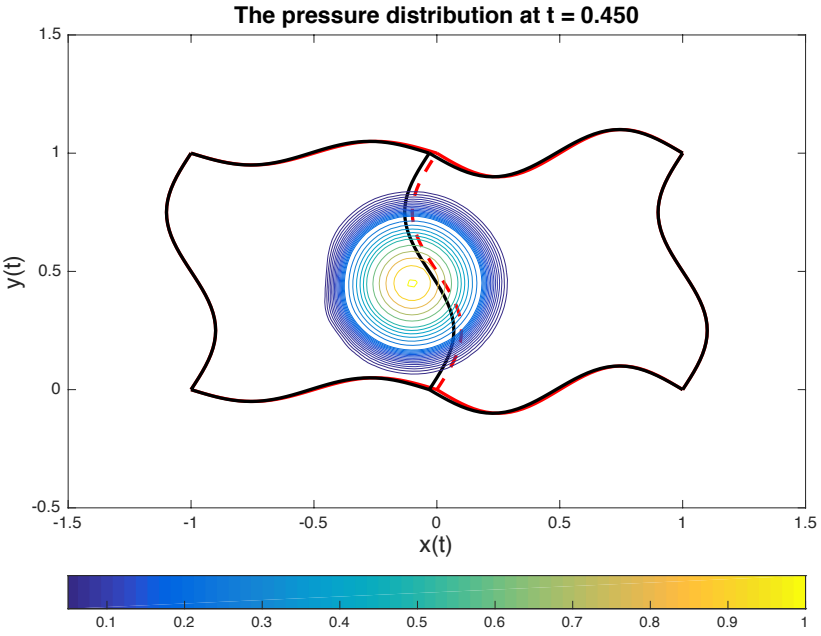

Figure 7: The pressure distribution.

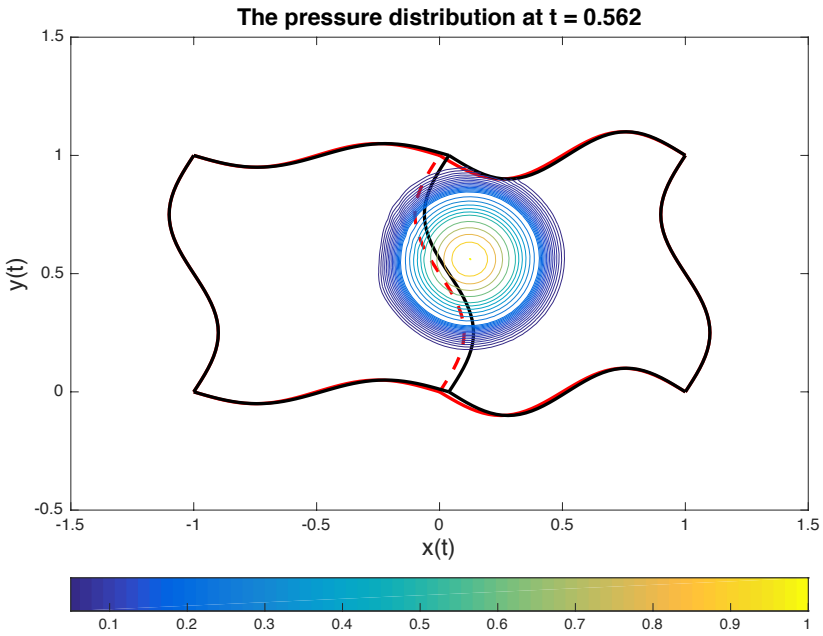

Figure 8: The pressure distribution.

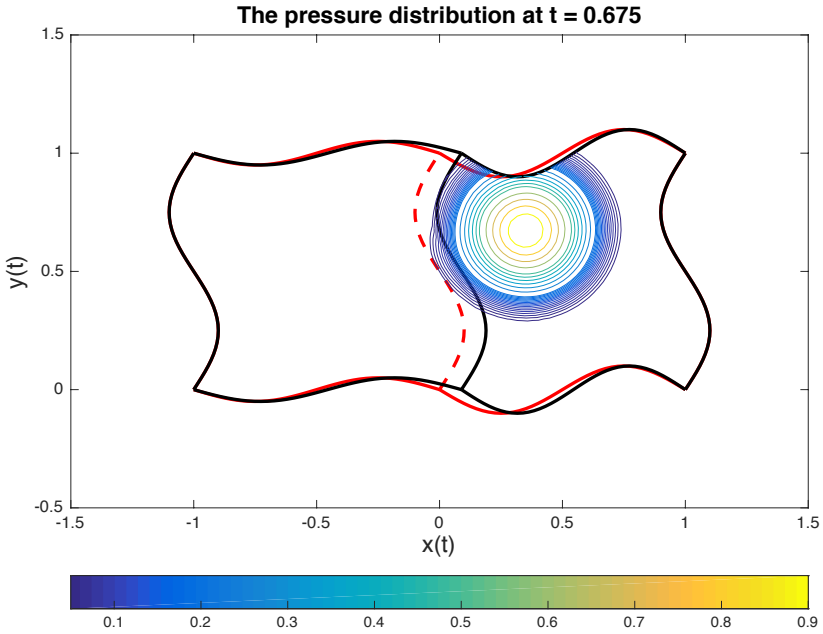

Figure 9: The pressure distribution.

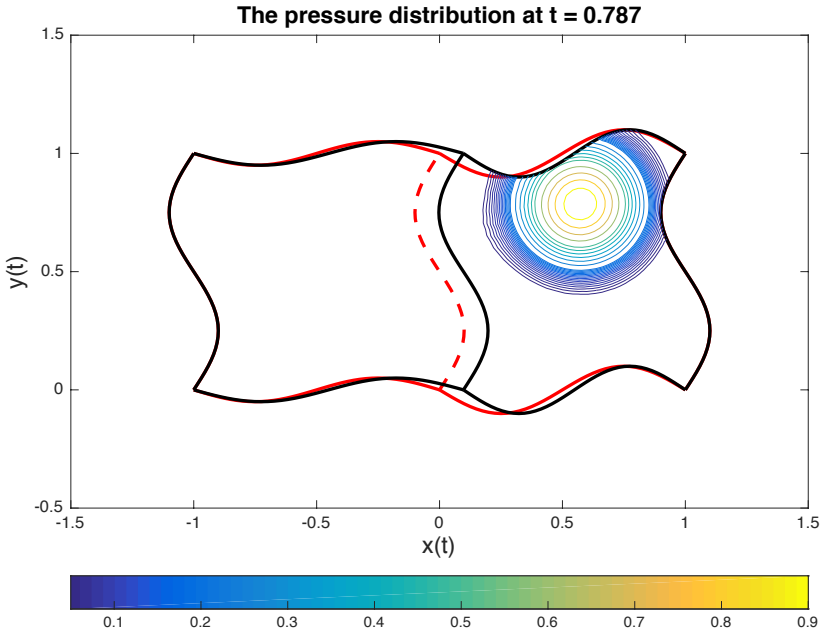

Figure 10: The pressure distribution.

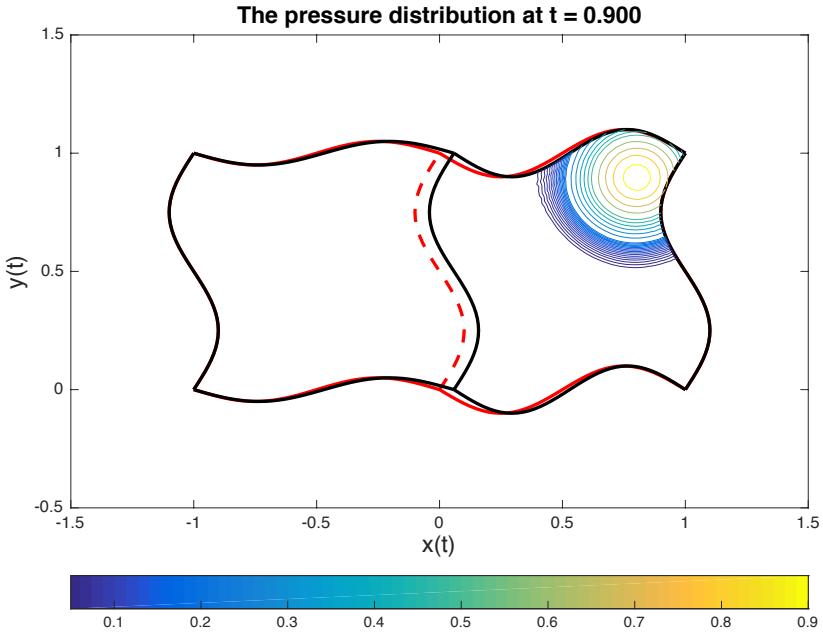

Figure 11: The pressure distribution.

REFERENCES

[1] S. Nikkar and J. Nordström, Fully discrete energy stable high order

finite difference methods for hyperbolic problems in deforming domains, *Journal of Computational Physics*, **291**:82-98 (2015).

[2] M. Svärd and J. Nordström, Review of summation-by-parts schemes for initial-boundary-value problems, *Journal of Computational Physics*, **268**:17-38, (2014).

[3] J. Nordström and J. Gong and E. van der Weide and M. Svärd, A stable and conservative high order high order multi-block method for the compressible Navier-Stokes equations, *Journal of Computational Physics*, **228**:9020-9035 (2009).

[4] Strand B., Summation by parts for finite difference approximations of d/dx, *Journal of Computational Physics*, **110**:47-67 (1994).

[5] J. Gong and J. Nordström, Interface procedures for finite difference approximations of the advection-diffusion equation, *Journal of Computational and Applied Mathematics*, **236**:602-620 (2011).

[6] K. Mattsson and M. H. Carpenter, Stable and Accurate interpolation operators for high-order multi-block finite-difference methods, *SIAM Journal of Scientific Computing*, **32**(4):22982320 (2010).

[7] Nordström J. and Lundquist. T., Summation-by-parts in time, *Journal of Computational Physics*, **251**:487-499 (2013).

[8] Lundquist, T. and Nordström, J., The SBP-SAT technique for initial value problems, *Journal of Computational Physics*, **270**:86-104 (2014).

[9] Svärd, M. Nordström, J., On the order of accuracy for difference approximations of initial boundary value problems, *Journal of Computational Physics*, **218**:333-352 (2006).

[10] Carpenter M. H., Nordström, J., Gottleib D., A Stable and Conservative Interface Treatment of Arbitrary Spatial Accuracy, *Journal of Computational Physics*, **148**:341-365 (1999).

[11] Carpenter M. H., Nordström, J., Gottleib D., Revising and extending interface penalties for multi-domain summation-by-parts operators, *Journal of Scientific Computing*, **45**:118-150 (2010).

[12] C. Farhat, P. Geuzaine, C. Grandmont, The discrete geometric conservation law and the nonlinear stability of ALE schemes for the solution of flow problems on moving grids, *Journal of Computational Physics*, **291**:82-98 (2015).

[13] S. Nikkar and J. Nordström, Fully discrete energy stable high order finite difference methods for hyperbolic problems in deforming domains, *Journal of Computational Physics*, **291**:82-98 (2015).

[14] Charles F. Van Loan, The ubiquitous Kronecker product, *Journal of Computational and Applied Mathematics*, **123**:85-100 (2000).

[15] Saul S. Abarbanel and Alina E. Chertock, Strict stability of high-order compact implicit finite-difference schemes: the role of boundary conditions for hyperbolic PDEs, I, *Journal of Computational Physics*, **160**(1):42-66 (2000).

[16] Mark H. Carpenter and David Gottlieb, Spectral Methods on Arbitrary Grids, *Journal of Computational Physics*, **129**:74-86, (1996).

[17] David C. Del Rey Fernández and Pieter D. Boom and David W. Zingg, A generalized framework for nodal first derivative summation-by-parts operators, *Journal of Computational Physics*, **266**:214-239 (2014).

[18] Saul S. Abarbanel and Alina E. Chertock and Amir Yefet, Strict stability of high-order compact implicit finite-difference schemes: the role of boundary conditions for hyperbolic PDEs, II, *Journal of Computational Physics*, **160**:67-87 (2000).

[19] Nordström, J., Conservative finite difference formulations, variable coefficients, energy estimates and artificial dissipation, *Journal of Scientific Computing*, **29**:375-404 (2006).

[20] Turkel, E., Symmetrization of the fluid dynamics matrices with applications, *Mathematics of Computation*, **27**:729-736 (1973).

[21] B. Gustafsson, H.-O. Kreiss, and J. Oliger, Time dependent problems and difference methods, John Wiley & Sons, New York, 1995.

[22] C.W Hirt and A.A Amsden and J.L Cook, An arbitrary Lagrangian-Eulerian computing method for all flow speeds, *Journal of Computational Physics*, **14**(3):227-253 (1974).

[23] Y. Abe and T. Nonomura and N. Iizuka and K. Fujii, Conservative metric evaluation for high-order finite-difference schemes with the GCL identities on moving and deforming grids, *Journal of Computational Physics*, **232**:14-21 (2013).

[24] K. Mattsson and M. H. Carpenter, table and accurate interpolation operators for high-order multiblock finite difference methods, *SIAM Journal on Scientific Computing*, **32**:2298-2320 (2010).

[25] T. Lundquist and J. Nordström, On the Suboptimal Accuracy of Summation-by-parts Schemes with Non-conforming Block Interfaces, *LiTH-MAT-R–2015/16–SE*.